ARTICLE

BIOTECHNOLOGY and BIOENGINEERING

Processing/Structure/Property Relationship of Multi-Scaled PCL and PCL–HA Composite Scaffolds Prepared via Gas Foaming and NaCl Reverse Templating

A. Salerno,[1,2] S. Zeppetelli,[2] E. Di Maio,[3] S. Iannace,[2] P.A. Netti[1,3]

[1]Interdisciplinary Research Centre on Biomaterials (CRIB), Italian Institute of Technology (IIT), University of Naples Federico II, Piazz.le Tecchio 80, 80125 Naples, Italy; telephone: +390817682536; fax: +390817682408; e-mail: asalerno@unina.it

[2]Institute of Composite and Biomedical Materials and National Research Council (IMCB-CNR), University of Naples Federico II, Piazz.le Tecchio 80, 80125 Naples, Italy

[3]Department of Materials and Production Engineering (DIMP), University of Naples Federico II, Piazz.le Tecchio 80, 80125 Naples, Italy

Received 10 August 2010; revision received 1 November 2010; accepted 2 November 2010

Published online 1 December 2010 in Wiley Online Library (wileyonlinelibrary.com). DOI 10.1002/bit.23018

ABSTRACT: In this study, we investigated the processing/structure/property relationship of multi-scaled porous biodegradable scaffolds prepared by combining the gas foaming and NaCl reverse templating techniques. Poly(ε-caprolactone) (PCL), hydroxyapatite (HA) nano-particles and NaCl micro-particles were melt-mixed by selecting different compositions and subsequently gas foamed by a pressure-quench method. The NaCl micro-particles were finally removed from the foamed systems in order to allow for the achievement of the multi-scaled scaffold pore structure. The control of the micro-structural properties of the scaffolds was obtained by the optimal combination of the NaCl templating concentration and the composition of the CO_2–N_2 mixture as the blowing agent. In particular, these parameters were accurately selected to allow for the fabrication of PCL and PCL–HA composite scaffolds with multi-scaled open pore structures. Finally, the biocompatibility of the scaffolds has been assessed by cultivating pre-osteoblast MG63 cells in vitro, thus demonstrating their potential applications for bone regeneration.

Biotechnol. Bioeng. 2011;108: 963–976.

KEYWORDS: gas foaming; hydroxyapatite; poly(ε-caprolactone); pore structure; scaffold; tissue engineering

Introduction

In the past two decades, the possibility of repairing and/or regenerating damaged or malfunctioning biological tissues by using porous scaffolds has been the subject of extensive efforts in the field of tissue engineering (TE). In fact, in the TE approach, the scaffold plays a pivotal role in guiding cell functions during de-novo tissue formation, providing a 3D porous substrate for cell adhesion and extracellular matrix deposition, as well as for the transport of fluids, compulsory for cell survival and biosynthesis in three dimensions (Hutmacher, 2001; Sang and Bhatia, 2004).

The design of porous scaffolds characterized by well controlled pore size, shape, interconnectivity, and spatial distribution is essential for promoting the three-dimensional migration and proliferation of cells, as well as for inducing new-tissue vascularization (Aronin et al., 2009; Huang et al., 2006; Oh et al., 2007; Silva et al., 2006). For instance, it has been demonstrated that different tissues require different pore sizes for their regeneration and that the diameter of cells in suspension dictates the minimum pore size, which varies from one cell type to another (Aronin et al., 2009; Oh et al., 2007). Recently, results of in vitro and in vivo studies suggested that scaffolds characterized by pore structures at different size scales may improve the process of new-tissue regeneration (Karageorgiou and Kaplan, 2005; Salerno et al., 2009; Silva et al., 2006). In particular, it has been demonstrated that, in the case of bone regeneration, a macro-porosity of the order of hundreds of microns is necessary to promote the in vitro cell invasion and differentiation, as well as the in vivo infiltration of the surrounding tissue (Karageorgiou and Kaplan, 2005; Salerno et al., 2009; Silva et al., 2006). Furthermore, the presence of a micro-porosity pathway, with pore size ranging from 1 to 50 microns, may promote the transport of fluids to the cell and tissue located within the interior of the

Correspondence to: A. Salerno

pore structure of the cell/scaffold construct (Karageorgiou and Kaplan, 2005; Salerno et al., 2009).

Several approaches have been proposed to imprint porosity architectures at different size scales within biocompatible and biodegradable materials. The majority of these techniques are based on the combination of two different processes, each optimized for a formation of a porosity scale. For instance, reverse templating techniques, such as porogen leaching (PL), that may allow for the tight control of the macro-porosity network of the scaffolds, have been combined to phase separation (PS) from polymer/solvent solutions in order to enhance pore interconnectivity and to control the pore wall texture (Guarino et al., 2008a; Reverchon et al., 2008; Wei and Ma, 2004). To overcome the limitations related to the use of organic solvents, potentially harmful to cells, tissues and bioactive factors, PS from polymer/gas solution, such as gas foaming (GF) process, has been investigated in combination with PL techniques (Chen et al., 2006; Harris et al., 1998; Kim et al., 2006; Salerno et al., 2009). Scaffolds prepared by this process are typically characterized by well controlled open pore networks and improved cell adhesion and new-tissue formation, both in vitro and in vivo (Harris et al., 1998; Kim et al., 2006; Salerno et al., 2009). Although the great advantage of the GF/PL combined process, the strong interdependence between the two different techniques requires a careful investigation of the processing/structure/property relationship with respect to the specific system selected. This aspect is very important to achieve a fine control of the micro-structural properties of the scaffold and, therefore, for the success of any TE scaffold application/strategy.

This study aims to provide new insights in the processing/structure/property relationship of poly(ε-caprolactone) (PCL) and PCL–hydroxyapatite (HA) nano-composite scaffolds prepared by combining GF and PL processes. PCL was mixed to HA nano-particles, in concentration from 5 to 20 wt%, to prepare biocompatible nano-composites for bone TE. The as-obtained biomaterials were mixed with NaCl micro-particles, in concentration ranging from 85 to 95 wt% and, subsequently, processed by GF. The effect of NaCl concentration and GF parameters on the pore structure of the scaffolds was surveyed, and the results correlated to the viscoelastic properties of the PCL and PCL–HA composite melt, with the ultimate goal to design porous scaffolds with multi-scaled pore size distributions. Finally, the biocompatibility of the scaffolds was assessed in vitro by using pre-osteoblast MG63 cells, to evaluate their potentials for bone TE applications.

Experimental

Materials

PCL ($M_W = 65$ kDa, $T_M = 59$–64°C and $\rho = 1.145$ g/cm^3) was purchased from Sigma–Aldrich (Milano, Italy). HA nano-particles (Berkeley Advanced Biomaterials Inc., Berkeley, CA, size 100 nm) were used for the preparation of the PCL–HA composites. NaCl micro-particles (J.T. Beker, Italy) were sieved to obtain 300–500 μm size particles and used as micro-particulate templating agent.

Methods

As schematically illustrated in Figure 1, the GF/PL combined technique is characterized by three different steps: mixing, foaming, and leaching.

Mixing

PCL pellets were melt-mixed with the HA nano-particles in an internal mixer (Rheomix® 600, Haake, Karlsruhe, Germany) controlled by a measuring drive unit (Rheocord® 9000, Haake) at 70°C, 100 rpm for 10 min. HA concentrations equal to 5 and 20 wt% were selected for the preparation of the PCL–HA_5 and PCL–HA_{20} composites, respectively. Neat PCL was subjected to the same mixing process for proper comparison. The PCL, PCL–HA_5, and PCL–HA_{20} biomaterials were then melt-mixed with the NaCl micro-particles by using the same mixing equipment and selecting three concentrations: 85, 90, and 95 wt%. Mixing temperature, speed, and time were settled to 130°C, 20 rpm, and 10 min, respectively, in order to preserve the size and shape of the NaCl crystals during the process. After mixing, the systems were compression moulded into 3 mm-thick plates by a hot press (P 300 P, Collin, Ebersberg, Germany) at 130°C and 0.3 MPa.

Foaming

Foaming experiments were carried out by solubilizing the samples with the blowing agent at 70°C and at saturation pressures in the range from 10 to 18 MPa for 4 h. The temperature was then cooled to 35°C and the pressure fast quenched to the ambient (1–2 s) to allow for gas bubbles nucleation and growth. Table I reported the details of the GF experiments performed, showing that different blowing agent mixtures, obtained by changing the CO_2–N_2 vol% composition in the range from 20–80 to 100–0, were selected to control foaming. Indeed, due to the plasticizing effect of CO_2 (Salerno et al., 2007), we increased the CO_2 amount in the blowing agent mixture to promote PCL foaming, especially at the highest NaCl and HA concentrations.

NaCl Leaching

The foamed samples were finally soaked in dH_2O under stirring at room temperature (RT) for 2 weeks to dissolve the NaCl particles and to obtain the final scaffold pore structure.

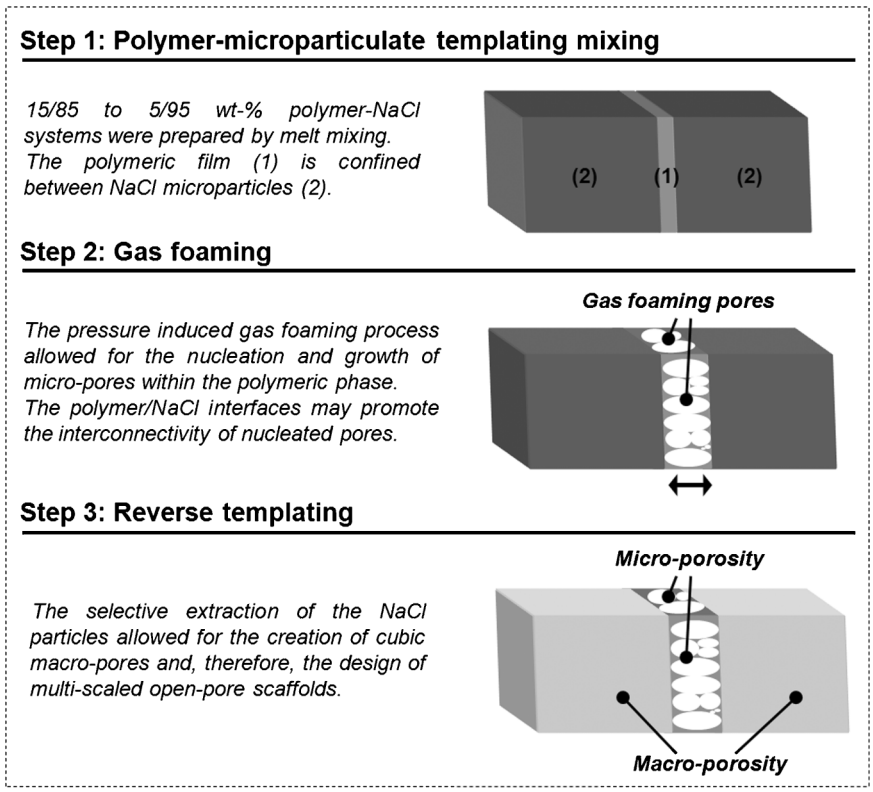

Figure 1. Scheme of the GF/PL three-step process: (**1**) PCL and PCL–HA composites were mixed with NaCl particles in composition ranging from 15/85 to 5/95 wt%, respectively; (**2**) the systems were subsequently subjected to the pressure-quench GF process in order to create the micro-porosity pathway within the polymer phase; and (**3**) the NaCl particles were finally removed from the foamed samples to allow for the formation of the macro-porosity network.

Characterization

Thermo-gravimetric (TGA) and derivative TGA (DTGA) analyses were carried out on both PCL and PCL–HA composites to assess their thermal stability and to quantify the effective HA amount. A TGA 2950 (TA Instruments, Milano, Italy) was used for the tests and the samples were analyzed from 30 to 500°C at 10°C/min under inert atmosphere.

The viscoelastic properties of PCL and PCL–HA composites were evaluated by using a strain controlled rotational rheometer (ARES L.S., Rheometric Scientific™, Milano, Italy) and the tests performed in parallel plates (25 mm diameter) geometry. Frequency scans were carried out from $\omega = 0.1$ to $\omega = 100$ rad/s at 90°C and with a 1% strain amplitude under inert atmosphere.

Table I. Processing conditions used for the design of the multi-scaled PCL and PCL–HA scaffolds.

Test	NaCl amount (wt%)	HA (wt%)	CO_2–N_2 (vol%)
1	85, 90, 95	0, 5, 20	20–80
2	85, 90, 95	0, 5, 20	40–60
3	90	5, 20	40–60
4	90	20	60–40
5	90	20	100–0

The morphology of the scaffolds was analyzed by SEM (S440, LEICA, Wetzlar, Germany) at an accelerating voltage of 20 kV, while gravimetric measurements and image analysis were used in order to evaluate the porosity and the pore size distribution of the scaffolds, as described in a previously reported work (Salerno et al., 2009).

The static compression properties of the scaffolds were determined by using an Instron mechanical testing system (4204, Instron, Milano, Italy), working at a cross head of 1 mm/min and equipped with a 1 kN loading cell. Five disc-shaped samples ($d = 10$ mm and $h = 4$ mm) were tested for each scaffold.

Energy Dispersive Spectroscopy (EDS, INCA 200, Oxford, UK) and trypan blue staining analyses were performed on PCL and PCL–HA composite scaffolds in order to assess their elemental composition and to examine the HA particles distribution and exposure on the pore walls of the scaffolds. For trypan blue staining, the scaffolds were soaked with a 1% w/v water solution for 10 min, washed twice in 100% ethanol and analyzed by an optical microscope (Kim et al., 2006).

The wettability of the scaffolds was evaluated by contact angle measurements on a Contact Angle System OCA20

(Dataphysics, Bergamo, Italy). A 3 μL water droplet was poured on the surface of the scaffolds and the contact angle was measured by SCA20 Software (Dataphysics). Forty measurements were performed for each scaffold type.

Cells Expansion, Seeding, and Culture

The biocompatibility of the scaffolds was assessed in vitro by using pre-osteoblasts MG63 cells. Cells were cultured in 75-cm^2 flask in α-Modified Eagle's Medium (α-MEM) (BioWittaker, Verviers, Belgium), containing 10% (v/v) FBS, 100 U/mL penicillin, and 0.1 mg/mL streptomycin (HyClone, Northumberland, UK) at 37°C and 5% CO_2. After washing with phosphate-buffered saline (PBS), cells were incubated with trypsin–EDTA (0.25% trypsin, 1 mM EDTA, Euroclone) for 5 min at 37°C. Scaffolds for cell culture experiments (7 mm in diameter and 4 mm thick) were sterilized by Gamma-irradiation at a dose of 2.5 Mrad for 8 min and at RT, and statically seeded with 5×10^4 cells/scaffold, re-suspended in 50 μL of medium. The cell/scaffold constructs were placed in 24-well culture plates and incubated for 2 h to allow for cell attachment. Subsequently, cell culture medium was added to each well to bring the total well volume to 1.5 mL. After 24 h of incubation, the medium was replaced with osteogenic differentiation medium (Sigma–Aldrich). The cell/scaffold constructs were cultured for 14 days by changing the cell culture medium every 3–4 days.

Cell/Scaffold Interaction Study

Cell viability and proliferation were evaluated by using Alamar Blue assay. The cell/scaffold constructs were removed from the culture plates at day 1, 3, 7, and 14, washed with PBS and placed into 24-well culture plates. DMEM (2 mL) medium without Phenol red (HyClone) containing 10% (v/v) Alamar Blue (Abd Serotec Ltd., Oxford, UK) were added to each well and the samples incubated for 4 h at 37°C and 5% CO_2. The solution was subsequently removed from the wells and analyzed by a spectrophotometer (multilabel counter, 1420 Victor, Perkin Elmer, Milano, Italy) at the wavelengths of 570 and 600 nm. The number of viable cells was assessed by comparing the absorbance values at different culture times with those of the calibration curve.

Cell morphology and distribution were investigated by SEM analysis. The cell/scaffold constructs were removed from the media, washed with PBS and fixed with 2.5% glutaraldehyde (Sigma–Aldrich) in 0.1 M Na-cacodylate (Carlo Erba, Milano, Italy) at pH 7.4. The constructs were subsequently dried overnight at RT and the seeding surfaces analyzed by SEM.

DNA/alkaline phosphatase activity (ALP) measurement, Alizarin Red Staining (ARS) and Osteopontin Immunofluorescence (OPN) analysis were used to evaluate the osteogenic expression of MG63. For the DNA/ALP test, the scaffolds were washed twice with ice cold PBS, transferred to centrifuge tubes containing 300 μL cell lysis buffer (BDBiosciences, Milano, Italy) and lysed at −4°C for 45 min. After 5 min of centrifugation, total amount of DNA was detected using Pico Green Assay (Molecular Probes, Milano, Italy), while ALP activity was measured using a biochemical assay (SensoLyte pNPP ALP assay kit, ANASPEC, Milano, Italy). Mineralized matrix synthesis was evaluated by osteogenesys assay ARS kit (Chemicon, Milano, Italy). At 14 days of culture the constructs were fixed with 4% paraformaldehyde solution for 20 min, rinsed three times with PBS and incubated with the dye for 30 min. The constructs were then washed three times with dH_2O, incubated with 10% acetic acid for 30 min and sonicated. After heating at 85°C for 10 min, the acidic supernatant pH was neutralized with 10% ammonium hydroxide. The optical density of the solution was analyzed by a spectrophotometer working at 405 nm. All of the analyses were performed in triplicate. For OPN analysis, the constructs were removed from the wells after 14 days of culture, fixed in 4% paraformaldehyde in 0.1 M PBS, pH 7.2, for 30 min at RT. After washing with PBS, the constructs were processed for immunofluorescence labeling and analyzed by a confocal laser scanning microscope (CLSM, LSM510; Zeiss). MG63 cultured on 2D culture plastics were used as control, and cultures performed in both standard (−OM) and osteogenic medium (+OM).

Statistical Analysis

The statistical significance of the results was assessed by one-way ANOVA. Tukey post-hoc test at the significance level $P < 0.001$ was used to identify statistically different groups by using Origin® software package.

Results

Thermal Degradation and Rheological Properties of PCL and PCL–HA Composites

Figure 2a reports the TGA/DTGA thermo-grams of PCL and PCL–HA composites. Curves evidence that all of the systems showed a single thermal degradation event in the 30–500°C temperature range. In particular, the DTGA results reported in the inset of Figure 2a more clearly indicated that the degradation temperature of the samples increases from 395.3°C for neat PCL to 401.1°C for PCL–HA_{20}. Furthermore, final residues at 500°C proved that the PCL quite completely degraded at 500°C, while for the PCL–HA_5 and PCL–HA_{20} composites residual weights equal to 6.5% and 19.4%, respectively, well matching the nominal HA concentration, were observed.

The frequency-dependence of G' and G'' moduli of neat PCL and PCL–HA composites are shown in Figure 2b and c. G'' of the neat polymer is higher than G' in the whole range of frequencies investigated and both moduli approached the terminal behavior, $G' \sim \omega^2$ and $G'' \sim \omega$, at low frequencies. Furthermore, we observed a monotonic increase of the

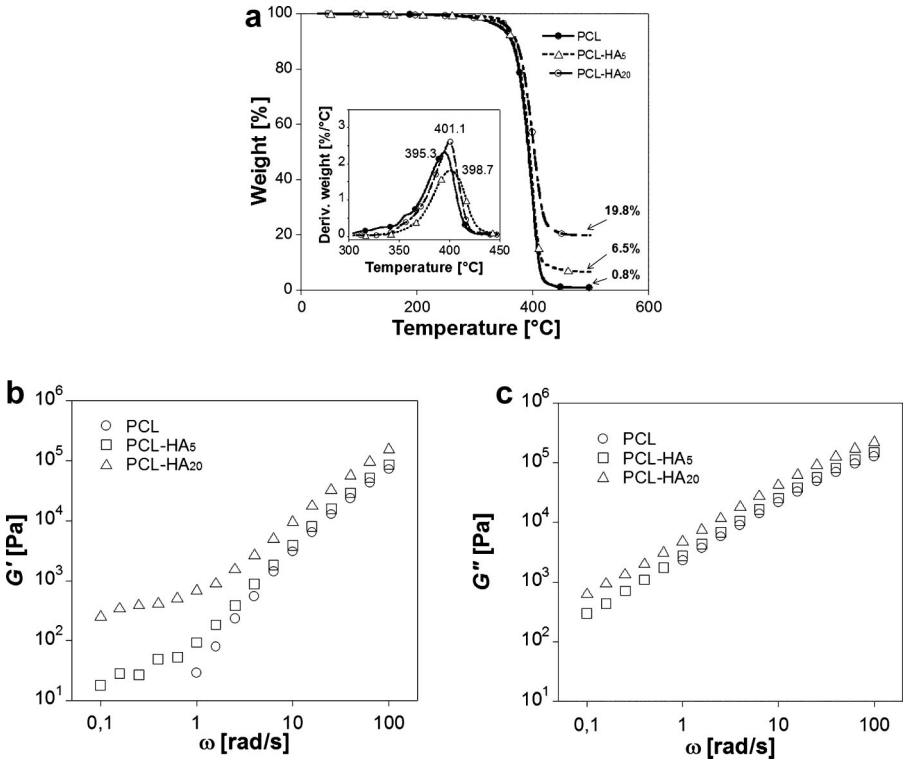

Figure 2. (**a**) TGA–DTGA results of neat PCL and PCL–HA composites; results of the rheological characterization of PCL and PCL–HA composites: (**b**) G' and (**c**) G'' versus ω curves.

moduli with increasing the HA concentration and a yield stress in the G' curves of the composites at low frequencies (Fig. 2b).

Design of Multi-Scaled PCL and PCL–HA Composite Scaffolds

Figure 3 reports SEM micrographs of the scaffolds before (Fig. 3a–c) and after (Fig. 3d–i) the GF step. As evidenced by the SEM images, the scaffolds were characterized by pore structures that well replicate the size and shape of the original NaCl particles. Nevertheless, the scaffolds prepared by the PL alone showed a porous structure with almost intact pore walls, proving very limited contact points between adjacent NaCl crystals in the polymer network (insets of Fig. 3a–c). This effect was mainly observed especially at the lower NaCl concentrations used. Conversely, the increase of the NaCl amount up to 95 wt% resulted in the increase of both scaffold porosity and interconnectivity, and also induced the formation of more irregular morphologies (compare Fig. 3a–c). Figure 3d–i shows the morphologies of the scaffolds prepared by combining the GF and PL processes (details of gas foaming experiments are reported in Table I). Differently from the mono-modal morphology of the scaffolds prepared by the PL alone, the scaffolds prepared by the GF/PL combined technique were characterized by multi-scaled morphologies. In particular, the GF step allowed for the formation of a micro-porosity pathway within the polymeric phase surrounding the NaCl particles, the extent and distribution of the micro-porosity decreasing with the increase of the NaCl concentration up to 95 wt%. It is, however, important to point out that the micro-porosity size and distribution increased with the increase of the CO_2 amount of the blowing agent mixture from 20 (#1) to 40 vol% (#2), this effect being more evident at lower NaCl concentrations (Fig. 3d, e, g, and h).

Figure 4a shows the porosity of the PCL scaffolds as function of NaCl concentration and foaming parameters. As expected, the overall porosity increased with the increase of the NaCl concentration for both PL and GF/PL scaffolds (Fig. 4a). Furthermore, a remarkable enhancement of the overall porosity of the scaffolds was also observed after the GF process, especially for the scaffolds prepared at the highest CO_2 concentration. For instance, the PCL scaffolds prepared by using 85 wt% of NaCl particles were characterized by an increase of the overall porosity from 75.7% (PL) to 83.4% (GF/PL, test #2). In agreement with the morphological results of Figure 3, a minor increase of the porosity was observed after the GF step at the highest NaCl concentrations. Figure 4b reports the pore size distribution of the PL and GF/PL scaffolds prepared by using 85 wt% of NaCl particles. As shown, the PL scaffold was characterized

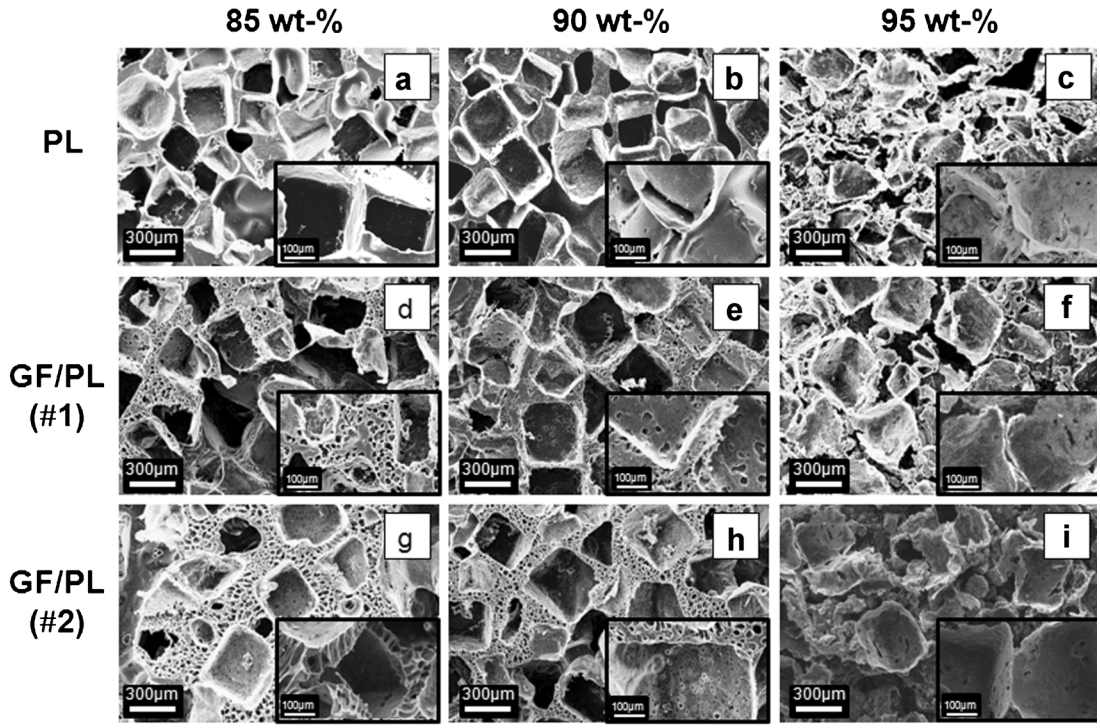

Figure 3. SEM micrographs of PCL scaffolds prepared as follows: PL PCL scaffolds prepared by using (**a**) 85, (**b**) 90, and (**c**) 95 NaCl wt%. GF/PL scaffolds prepared by using the processing conditions of test #1 and a NaCl wt% equal to (**d**) 85, (**e**) 90, and (**f**) 95. GF/PL scaffolds prepared by using the processing conditions of test #2 and a NaCl wt% of (**g**) 85, (**h**) 90, and (**i**) 95.

by a mono-modal pore size distribution, with pore sizes in the 200–600 μm range, well matching the optimal size of the NaCl particles used. Conversely, multi-scaled pore size distributions were observed for the GF/PL scaffolds, these scaffolds being characterized by a micro-porosity in the 20–100 μm range and a macro-porosity in the 200–600 μm range. Furthermore, the macro-porosity fraction and size increased with the increase of the CO_2 concentration of the blowing agent mixture from 20 (#1, Table I) to 40 vol% (#2, Table I). Figure 4c reports the results of the mechanical characterization of the PCL scaffolds. As shown, the mechanical response of the scaffolds was strongly dependent on their overall porosity, with a the decrease of E with the increase of both NaCl concentration and CO_2 amount of the blowing agent mixture. In particular, the highest value of E, equal to 4.77 MPa, was achieved for the PL scaffold prepared by using 85 wt% of NaCl particles, while values as low as 0.4 MPa were observed for a concentration of NaCl equal to 95 wt%. Taking into the account all of these results, the effect of the HA nano-particles on the morphology, porosity and mechanical properties of the scaffolds was investigated by selecting 90 wt% of NaCl and performing the GF step with a 40–60 CO_2–N_2 blowing agent mixture. As shown in Figure 5, these scaffolds were characterized by multi-scaled pore size distributions. Nevertheless, different micro-porosity features were observed with respect to the different HA concentration used. In particular, if compared to the PCL–HA_{20} composite scaffold, neat PCL and PCL–HA_5 composite scaffolds were characterized by larger pores (compare Fig. 5a–c). Interestingly, the higher magnification of the micro-porosity of the PCL–HA_5 composite scaffold, reported in Figure 5d, evidenced a fibrillar morphology, typical of the highly interconnected foams prepared by the GF process (Salerno et al., 2008) with interdispersed HA particles (black arrow). Further foaming experiments were carried out to investigate the effect of the CO_2 concentration in the blowing agent mixture on the micro-porosity of the PCL–HA_{20} scaffold (tests #4 and #5 of Table I). Although higher CO_2 concentrations may be expected to enhance the foamability of the polymeric matrix (Salerno et al., 2007), minor differences in the morphology of the micro-porosity were observed for the different processing conditions used (data not shown). Therefore, we selected the multi-scaled PCL and PCL–HA_5 scaffolds of Figure 5a and b, for further characterizations.

The HA particles exposure was assessed by trypan blue staining and the EDS analysis and, the results reported in Figure 6. The staining test clearly demonstrated that the HA particles are exposed and uniformly distributed on the PCL–HA_5 scaffold surface (compare Fig. 6a and b), while the EDS analysis evidenced a Ca/P ratio of 1.76 (Fig. 6b), close to the stoichiometric HA composition (Guarino et al., 2008). The results of the contact angle tests, reported in Figure 6c indicated that the HA did not affect significantly

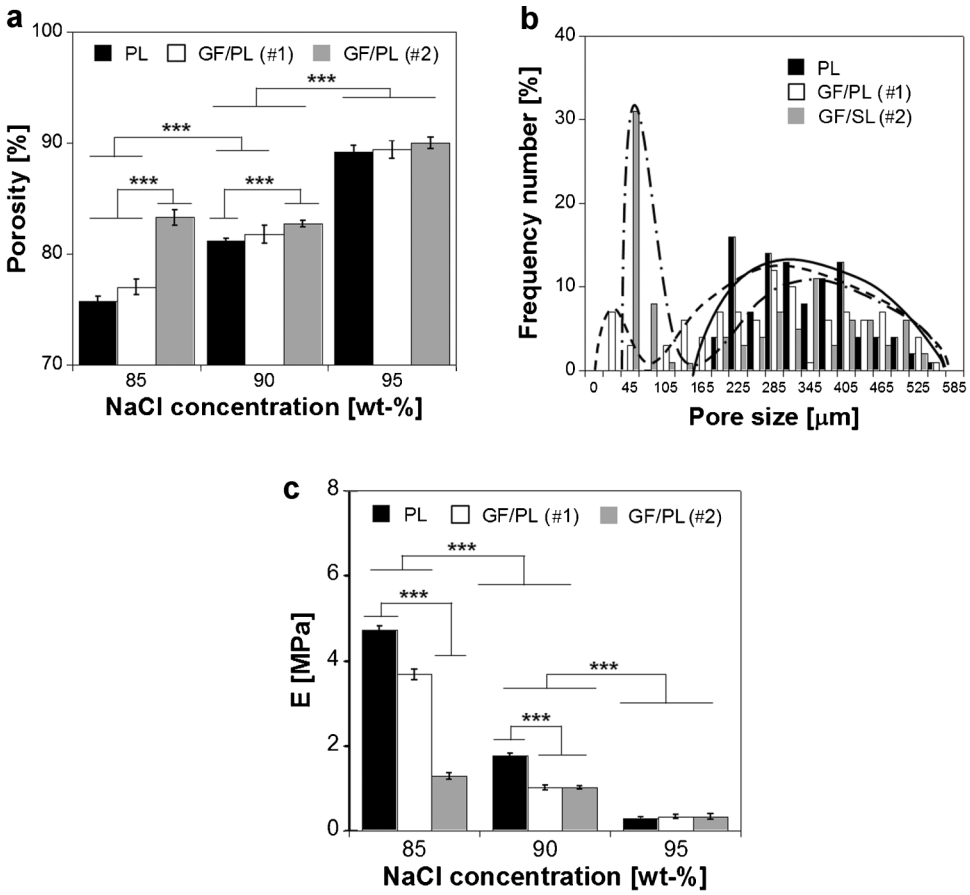

Figure 4. (**a**) Porosity of PCL scaffolds prepared by using different NaCl concentrations and GF parameters; (**b**) pore size distribution of PCL scaffolds prepared by using 85 wt% of NaCl and selecting different GF parameters; and (**c**) Effect of NaCl concentration and GF process parameters on *E* values of PCL scaffolds.

the wettability of the scaffolds, as evidenced by contact angle values of 103.1 ± 3.9 and to 104.1 ± 7.8 for neat PCL and PCL–HA_5 scaffold, respectively.

Cell/Scaffold Interaction Study

The multi-scaled PCL and PCL–HA_5 composite scaffolds were tested in vitro by using pre-osteoblasts MG63 cells to assess their potential for bone TE. Alamar Blue assay has been performed in order to evaluate cell viability and proliferation and the results reported in Figure 7a, along with those obtained for the MG63 cultured on 2D culture plastics. As shown, enhanced MG63 proliferation was observed on 2D culture plastics, as indicated by the increase of the number of viable cells from $0.90 \times 10^5 \pm 0.11 \times 10^5$ at day 1 to $5.72 \times 10^5 \pm 0.31 \times 10^5$ at day 14. When cultured within the PCL and PCL–HA_5 porous scaffolds, the MG63 were characterized by similar proliferation trends, with the number of viable cells that increased from $0.37 \times 10^5 \pm 0.19 \times 10^5$ and $0.60 \times 10^5 \pm 0.07 \times 10^5$ at day 1 to $2.20 \times 10^5 \pm 0.42 \times 10^5$ and $2.81 \times 10^5 \pm 0.47 \times 10^5$ at day 14 for neat PCL and PCL–HA_5 composite scaffolds, respectively. Figure 7b–e showed the morphology and distribution of the MG63 on the seeding surface of the cell/scaffold constructs after 1 and 14 days of in vitro culture. At day 1 (Fig. 7b and c), the cells colonized the surface of the scaffolds, preferentially adhering within the macro-porosity originated from the NaCl leaching. Furthermore, the higher magnifications of the insets of Figure 7b and c evidenced the good adhesion between cells and scaffold, and the formation of cell bridges between opposite pore walls. After 14 days of culture, cell proliferation resulted in the development of dense cell sheets covering the supporting scaffold architecture (Fig. 7d and e).

The osteogenic differentiation of the MG63 cells was assessed by ALP activity, ARS and immunofluorescence OPN tests. As shown in Figure 8a, the ALP activity of the osteogenically induced MG63 cells cultured within the PCL and PCL–HA_5 scaffolds was equal to 0.050 ± 0.021 and 0.051 ± 0.016, respectively at day 7. A significantly lower value ($P < 0.001$), equal to 0.007 ± 0.003, was observed for the 2D culture. The cells cultured on 2D plastics evidenced an increase of their ALP activity up to one order of magnitude from day 7 to 14 (0.093 ± 0.008), while a minor decrease was observed at the same culture time for the cells

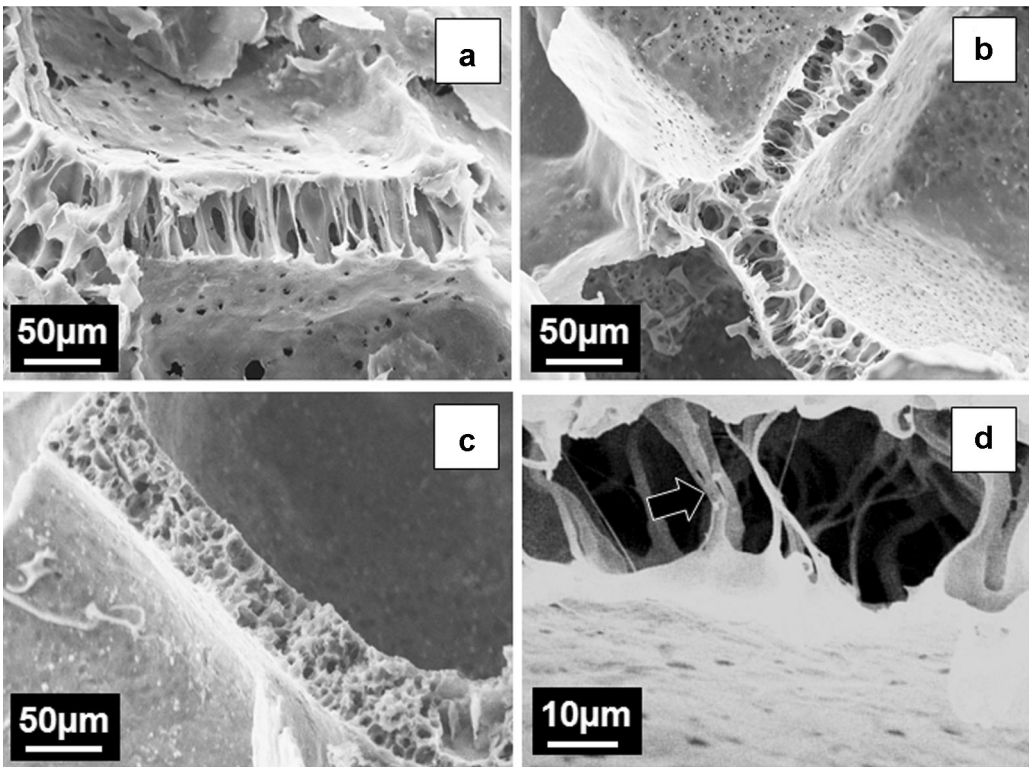

Figure 5. SEM micrographs of porous scaffolds prepared in the test conditions #2 and by using different HA concentrations: (**a**) neat PCL, (**b**) and (**d**) PCL–HA_5, (**c**) PCL–HA_{20}. The black arrow in (d) indicated the HA particles in the foamed polymer.

cultured within porous scaffolds (0.030 ± 0.014 for PCL and 0.023 ± 0.005 for PCL–HA_5 scaffold, respectively, as shown in Fig. 8a). The results of the ARS analysis performed on the porous scaffolds after 14 days of culture, reported in Figure 8b, also show a similar amount of calcium deposited by the cells cultured within the porous PCL and PCL–HA_5 composite scaffolds. The results of the immunofluorescent staining of OPN confirmed the osteogenic expression of the MG63 cells on both the seeding surface (Fig. 9c and d) and within the interior of the PCL and PCL–HA_5 composite scaffolds (Fig. 9e–h).

Discussion

Design of Multi-Scaled PCL and PCL–HA Composite Scaffolds

Porous biodegradable scaffolds are widely used in TE to provide a 3D substrate for cell attachment, proliferation, and differentiation in vitro, and to guide the process of new-tissue regeneration in vivo (Aronin et al., 2009; Hutmacher, 2001; Oh et al., 2007; Sang and Bhatia, 2004). Recently, the design of porous scaffolds with multi-scaled pore structures has been indicated as one of the most efficient strategies to improve the new-tissue regeneration process (Guarino et al., 2008a; Salerno et al., 2009; Silva et al., 2006; Sosnowski et al., 2006; Vidaurre et al., 2007). In particular, it has been reported that the presence of a macro-porosity network may allow for an efficient cell colonization and infiltration in 3D, while a micro-porosity pathway may promote the diffusion of nutrients, metabolic wastes, and degradation products, to and from the interior of the cell/scaffold construct (Salerno et al., 2009; Silva et al., 2006; Sosnowski et al., 2006). In this work, we investigated the processing/structure/property relationship of PCL and PCL–HA composite scaffolds prepared by combining GF and PL, finally aiming to designing multi-scaled porous scaffolds for bone TE. To this ultimate goal, the scaffolds were characterized to assess the in vitro adhesion, proliferation, and osteogenic differentiation of pre-osteoblast MG63 cells.

As reported in the scheme of Figure 1, the multi-scaled scaffolds were designed and produced by the GF/PL combined process. This process allowed for the tight control of the macro-porosity, by the appropriate selection of the NaCl particles size and concentration, as well as the control of the micro-porosity, by the modulation of the GF parameters (Figs. 3 and 4). Although several studies investigated the design and fabrication of porous scaffolds by this combined technique (Chen et al., 2006; Harris et al., 1998; Kim et al., 2006; Salerno et al., 2009), to date very little is known about the processing/structure/properties relationship of PCL and PCL–HA nano-composite scaffolds prepared by this combined process (Salerno et al., 2008).

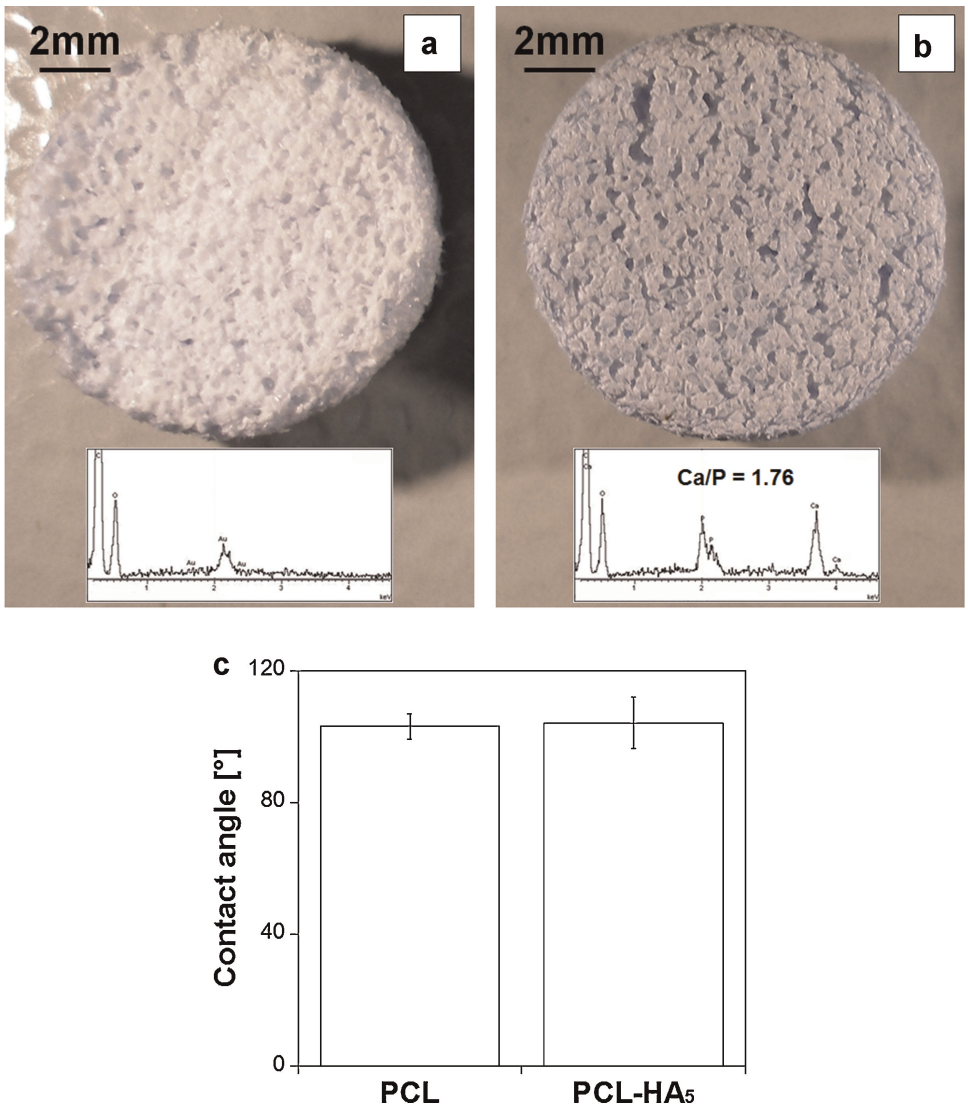

Figure 6. Results of the EDS analysis and HA particles staining by trypan blue test: (**a**) neat PCL and (**b**) PCL–HA_5. (**c**) Contact angle measurements on PCL and PCL–HA_5 scaffolds.

The microstructure of the scaffolds that can be designed with the GF/PL combined technique strongly depends on several factors, related to the materials and the processes involved. In particular, the macro-porosity depends on the NaCl concentration and size, that have been selected in the range from 85 to 95 wt% and 300–500 μm, respectively, in agreement with previous literature studies (Chen et al., 2006; Guarino et al., 2008; Harris et al., 1998; Kim et al., 2006; Vidaurre et al., 2007). Furthermore, the micro-porosity depends on the nucleation and growth of gas bubbles within the polymer phase during the GF process, in turn affected by the blowing agent composition and NaCl particles concentration. The SEM micrographs reported in Figures 3 and 5 demonstrated that the GF/PL process allowed for the design of multi-scaled porous PCL and PCL–HA composite scaffolds with well-controlled pore structures. In particular, if compared to the scaffolds prepared by the PL alone (Fig. 3a–c), those prepared by the combined technique evidenced an homogeneous distribution of the micro-porosity that is expected to allow for a more efficient 3D diffusion of the fluids and degradation products (Guarino et al., 2008; Sosnowski et al., 2006). The results of the experimental investigation performed in this study also indicated that the topological properties of the micro-porosity of the scaffolds may be efficiently modulated by the appropriate combination of both NaCl concentration and blowing agent composition. Indeed, enhanced foamability was obtained by the increase of the CO_2 in the blowing agent mixture from 20 (#1) to 40 vol% (#2) (Figs. 3 and 4a and b), as a consequence of the enhanced plasticization of the blowing agent mixture (Salerno et al., 2007). Scaffolds with different macro-porosity/micro-porosity fractions and

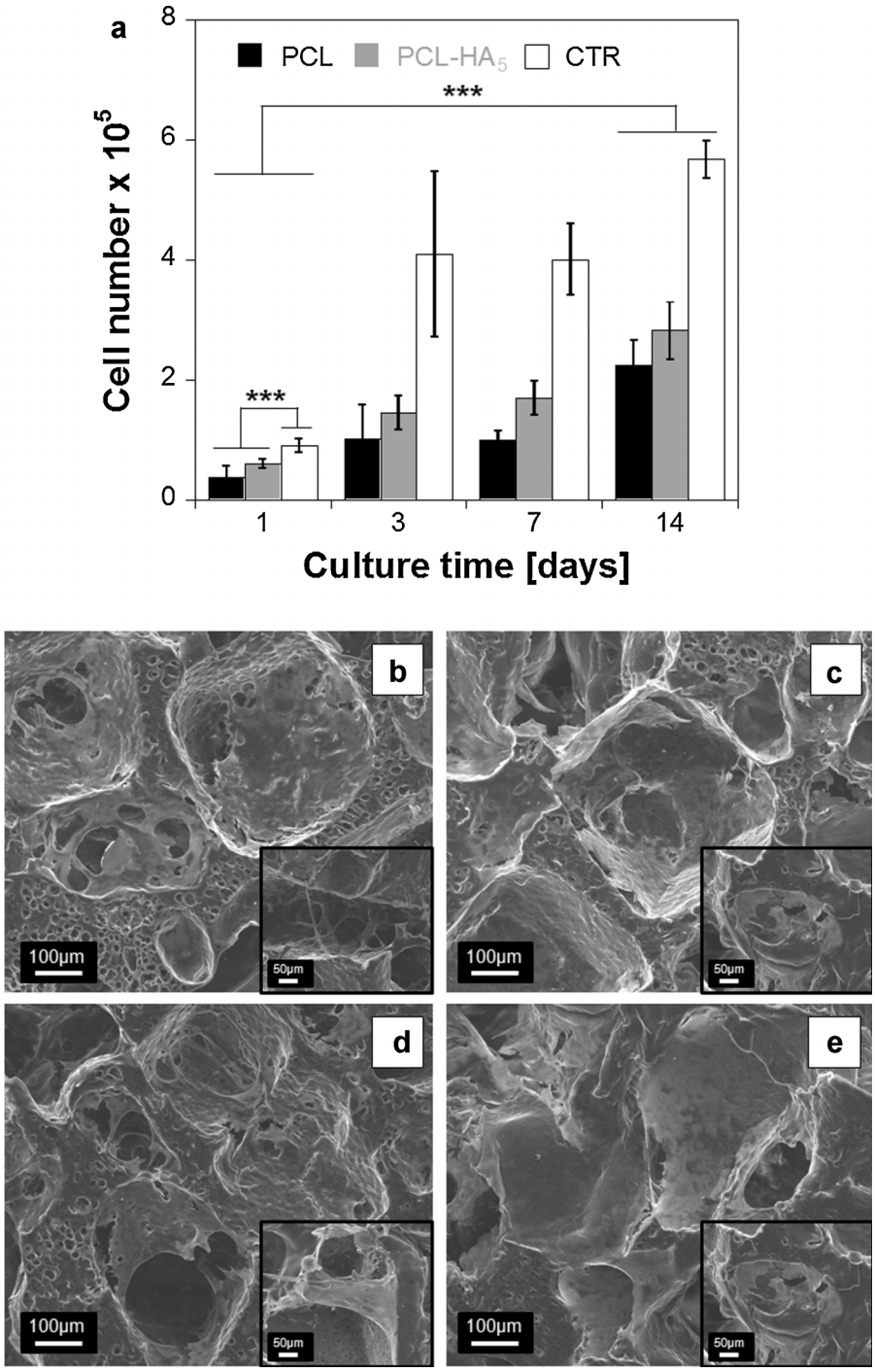

Figure 7. (**a**) MG63 viability and proliferation during 14 days of culture measured by Alamar Blue assay on culture plastics (CTR) and porous PCL and PCL–HA_5 scaffolds. SEM micrographs of the seeding surface of the cell/scaffold constructs at different culture time: (**b**) and (**d**) showed the MG63 cells onto the PCL scaffold a day 1 and 14 of culture, respectively; (**c**) and (**e**) showed the MG63 cells onto the PCL–HA_5 scaffold a day 1 and 14 of culture, respectively. Asterisks denote significant differences ($P < 0.001$) in cell number between different cell populations, as determined by Tukey post-hoc test.

micro-porosity dimensions were obtained, hence, by controlling the composition of the blowing agent mixture. Nevertheless, due to the interdependence between GF and PL processes, the size and extent of the micro-porosity decreased with the increase of the NaCl concentration. This effect was attributed to the decrease of the polymer amount and to the increase of the stiffness of the system with the NaCl concentration (Salerno et al., 2008).

Providing an adequate mechanical support is a very important TE scaffold requirement since they may affect cell behavior and biosynthesis as well as define suitable in vitro and/or in vivo applications (Hollister, 2005; Hutmacher,

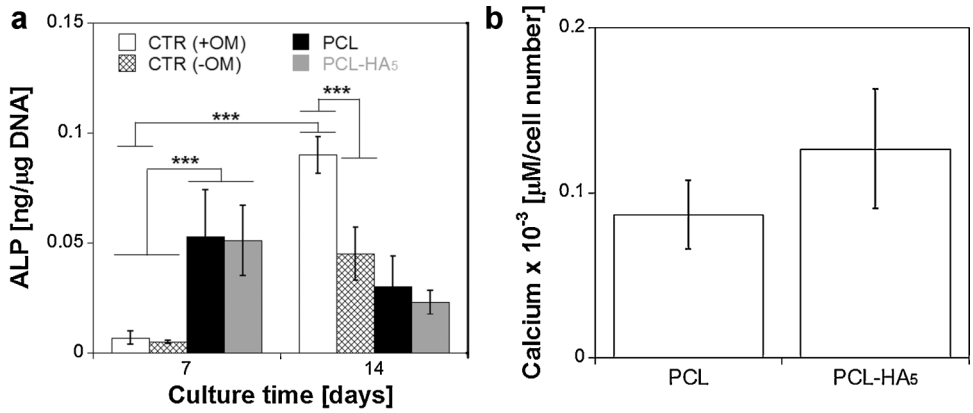

Figure 8. (**a**) Osteogenic differentiation of the MG63 cells measure by ALP/DNA assay at day 7 and 14 of culture; (**b**) mineralized matrix synthesis on the PCL and PCL–HA_5 scaffolds at 14 days of culture measured by ARS analysis. CTR cultures have been performed under standard (−OM) and osteogenic medium (+OM) for comparison. Asterisks denote significant differences ($P < 0.001$) in ALP activity between different cell populations and culture conditions, as determined by Tukey post-hoc test.

2001; Silva et al., 2006). As expected, we observed the decrease of *E* by increasing both NaCl concentration and CO_2 of the blowing agent mixture (Fig. 4c). Similar mechanical properties were reported by Lebourg et al. and Yao et al. for bTE PCL scaffolds with porosity in the range from 60% to 86% and prepared by using compression-molding and PL technique (Lebourg et al., 2008; Yao et al., 2006) and, by Guarino et al. for bTE PCL scaffolds prepared by PS and PL techniques (Guarino et al., 2008).

Further investigations have been performed in order to optimize the multi-scaled pore structure of PCL–HA composite scaffolds as a function of HA loading (experimental conditions are reported in Table I). In particular, to allow for the design of scaffolds with an adequate micro-porosity to macro-porosity fraction, we fixed the NaCl concentration to 90 wt% and selected different blowing agent mixtures. We observed that at the highest HA concentration the micro-porosity size and interconnection decreased (compare Fig. 5a–c), while foamability of the system was not significantly affected by the increase of the CO_2 concentration of the blowing agent mixture (data not shown). These results suggest the difficulty to control the foaming process for the high HA-loaded system, probably due to the increase of the stiffness of the polymeric matrix, as shown in Figure 2b, and also reported in literature for others polymeric composites (Lee et al., 2005; Salerno et al., 2008). Taking into the account all of these results, we further limited the wettability and in vitro biocompatibility characterizations to the PCL and PCL–HA_5 composite scaffolds prepared by the GF conditions of test #2 (Table I).

From a biological point of view, the exposure of the HA particles on the scaffolds pore walls is necessary to allow for an optimal interaction between the osteoinductive filler and bone cells (Guarino et al., 2008; Kim et al., 2006). As also reported by Kim et al. for poly(lactide-co-glycolide)/hydroxyapatite composite scaffolds (Kim et al., 2006) and evidenced by the results of EDS analysis and trypan blue test of Figure 6, the GF/PL process allowed for the extensive exposure of the HA nano-particles on the pore surface of the scaffold (Fig. 6b). Nevertheless, any significant differences were observed between the wettability of PCL and PCL–HA_5 scaffolds, despite the hydrophilicity of the HA, suggesting that at low HA concentration, the wettability was mainly dependent on the scaffolds topology.

Cell/Scaffold Interaction

The biocompatibility of the multi-scaled PCL and PCL–HA_5 scaffolds has been investigated in vitro by using pre-osteoblast MG63 cells. These cells are at a relatively early state in the osteoblastic lineage, and therefore may represent a good model for the examination of the initial stages in cell osteogenic differentiation induced by biomaterial scaffolds (Lampin et al., 1997). The results of the in vitro study are reported in Figures 7–9. The number of viable cells increased for both scaffolds from day 1 to 14 of culture (Fig. 7), even if a slightly higher number of viable cells was observed for the PCL–HA_5 scaffold. These results are in agreement with those reported in the literature on the ability of PCL and PCL–HA composite porous scaffolds to promote the in vitro adhesion and proliferation of pre-osteoblasts MG63 cells (Kweon et al., 2003; Oh et al., 2007; Ye et al., 2010). For instance, Ye et al. have recently reported that the extent of cell proliferation on PCL–HA composite scaffolds increased with the increase of the HA concentration (Ye et al., 2010). This effect was attributed to the enhancement of scaffold hydrophilicity and to the modification of the pore surface texture after the incorporation of the HA nano-particles. Although in our case we did not observe significant differences in the wettability of PCL and PCL–HA_5 composite scaffolds (Fig. 6c), the exposure of the HA nano-particles on the pore walls, as evidenced in Figures 5b and 6b, may affect slightly the MG63

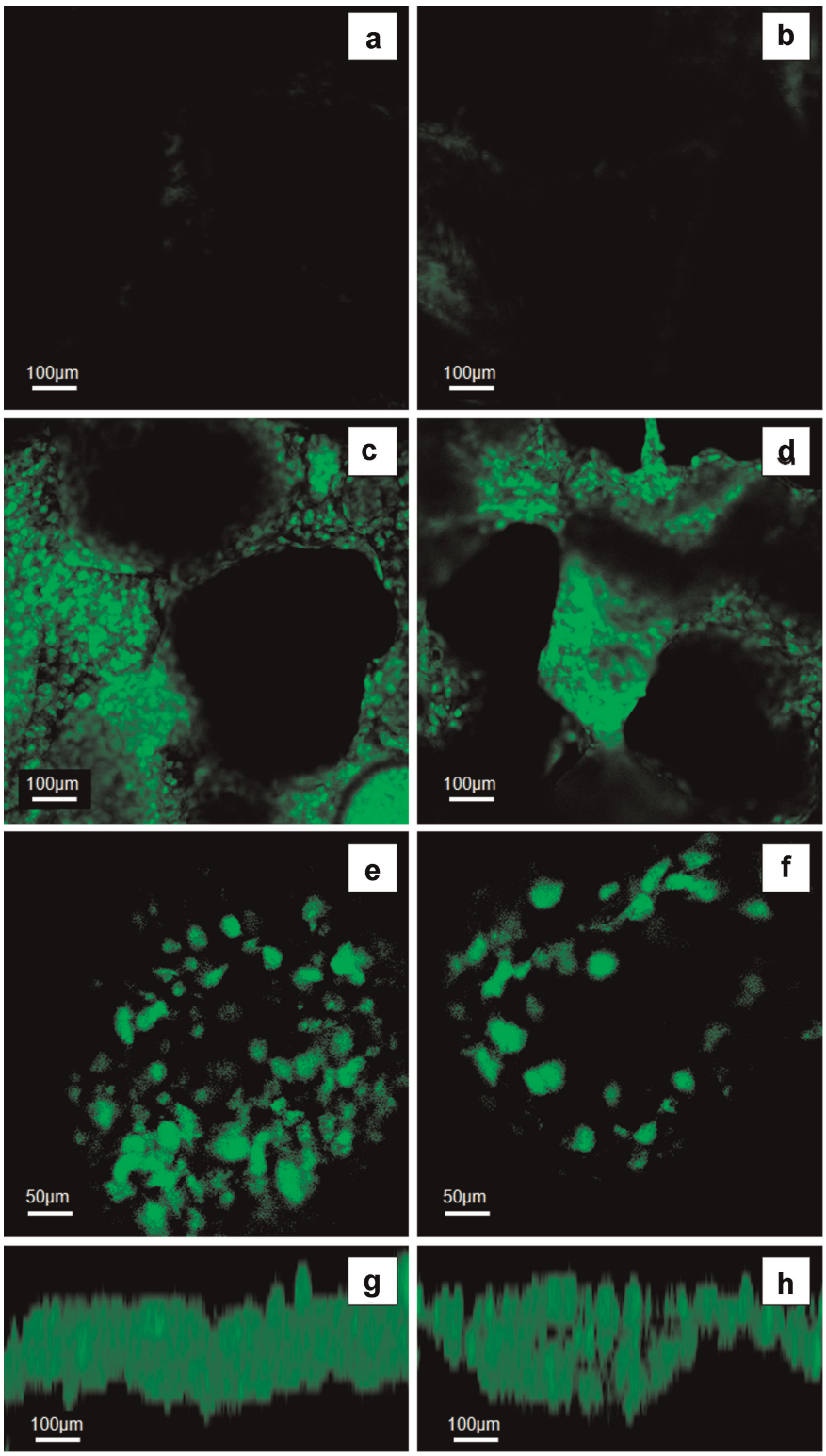

Figure 9. Immunostaining of osteopontin on the seeding surfaces of the PCL (**c**,**e**,**g**) and PCL–HA_5 (**d**,**f**,**h**) scaffolds at day 14 of culture. Unseeded PCL (**a**) and PCL–HA_5 (**b**) scaffolds are reported as control. [Color figure can be seen in the online version of this article, available at http://wileyonlinelibrary.com/bit]

proliferation. As expected, higher cell proliferation was observed for the 2D cultures (Fig. 7), this effect being probably due to the different cells/material interaction, as well as to the more efficient fluids exchange (Kweon et al., 2003). The ability of the porous scaffolds to allow for MG63 adhesion and proliferation was supported by the morphological characterization of the cell/scaffold constructs, reported in Figure 7b–e. These results evidenced the colonization of the cells within the macro-porosity of the scaffolds, and the formation of cell bridges between opposite pore walls (Fig. 7e–h). ALP, AR, and OPN tests were used as osteogenic markers to assess the bone regeneration potential of the multi-scaled PCL and PCL–HA_5 scaffolds prepared. As observed for the proliferation results, the ALP activity was significantly different between the 2D and 3D cultures, while minor differences were observed between the PCL and PCL–HA_5 porous scaffolds. In particular, our results indicated that the ALP activity of the osteogenically induced MG63 cells cultured within the scaffolds was higher at day 7 rather than day 14 (Fig. 8a). Conversely, when cultured on 2D culture plastics, the MG63 cells expressed very low ALP activity at day 7, while the ALP increased up to one order of magnitude after 14 days of culture. ALP is an early marker for the osteogenic differentiation of cells. The observed differences in ALP activity between 2D and 3D cultures suggested that the 3D porous PCL and PCL–HA_5 scaffolds induced a faster osteogenic differentiation of the MG63 cells, rather than the 2D culture plastics. There are several factors affecting the osteogenic differentiation of cells in vitro. Parameters such as materials chemistry and topography have been proved to significantly influence the osteogenic expression of different cell phenotypes (Guarino et al., 2008; Karageorgiou and Kaplan, 2005; Lange et al., 2002; Salerno et al., 2010). Similarly, seeding density and spatial distribution have also been indicated as key factors influencing the differentiation and extracellular matrix deposition by osteogenic induced cells in vitro (Lode et al., 2008). When cultured on 2D culture plates the MG63 evidenced a slight proliferation rate from 3 to 14 days of culture (Fig. 7a) and were induced to differentiate during this period as evidenced by the significant increase of the ALP from day 7 to 14. Conversely, slower proliferation rates were observed for the MG63 cultured within the porous scaffolds, this effect being also related to the faster osteogenic expression by the cell, as shown in Figure 8a. Usually, the decrease of the ALP activity of MG63 cells is associated to the expression of later-stage osteogenic markers and to the begin of calcium deposition (Yoshida et al., 2010). As shown in Figure 8b, the cells cultured within the PCL and PCL–HA_5 composite scaffolds expressed similar calcium contents after 14 days of culture, suggesting that higher HA amounts are required to enhance the deposited calcium at the early stages of in vitro MG63 culture (Guarino et al., 2008; Kim et al., 2006; Salerno et al., 2010). In agreement with the results of Figure 8, a similar expression of the osteopontin, a phosphoprotein that regulate the formation and remodeling of mineralized tissues, was observed after 14 days for the MG63 cultured within the PCL and PCL–HA_5 scaffolds (Fig. 9). Interestingly, the OPN immunostaining was observed on both seeding surfaces (Fig. 9c and d) and within the interior of the pore structure of the scaffolds (Fig. 9e–h). These results demonstrated the ability of the multi-scaled scaffolds to allow for the 3D osteogenic differentiation of MG63 cells.

Conclusions

In this study we investigated the processing/structure/properties relationship of multi-scaled PCL and PCL–HA composite scaffolds prepared via GF/PL combined technique. In particular, we reported that, by varying the NaCl concentration and the CO_2–N_2 blowing agent mixture composition it was possible to design PCL and PCL–HA composite scaffolds with multi-scaled pore size distributions and able to allow for the three-dimensional MG63 cells adhesion, proliferation, and osteogenic differentiation in vitro.

References

Aronin CEP, Sadik KW, Lay AL, Rion DB, Tholpady SS, Ogle RC, Botchwey EA. 2009. Comparative effects of scaffold pore size, pore volume, and total void volume on cranial bone healing patterns using microsphere-based scaffolds. J Biomed Mater Res A 89A:632–641.

Chen RR, Silva EA, Yuen WW, Mooney DJ. 2006. Spatio-temporal VEGF and PDGF delivery patterns blood vessel formation and maturation. Pharm Res 24:258–264.

Guarino V, Causa F, Netti PA, Ciapetti G, Pagani S, Martini D, Baldini N, Ambrosio L. 2008. The role of hydroxyapatite as solid signal on performance of PCL porous scaffolds for bone tissue regeneration. J Biomed Mater Res B: Appl Biomater 86B:548–557.

Guarino V, Causa F, Salerno A, Ambrosio L, Netti PA. 2008a. Design and manufacture of microporous polymeric materials with hierarchal complex structure for biomedical application. Mater Sci Tech 24: 1111–1117.

Harris DL, Kim B, Mooney DJ. 1998. Open pore biodegradable matrices formed with gas foaming. J Biomed Mater Res 42:396–402.

Hollister SJ. 2005. Porous scaffold design for tissue engineering. Nat Mater 4:518–524.

Huang Y, Siewe M, Madihally SV. 2006. Effect of spatial architecture on cellular colonization. Biotech Bioeng 93:64–75.

Hutmacher DW. 2001. Scaffold design and fabrication technologies for engineering tissues-state of the art and future perspectives. J Biomater Sci Polym Ed 12:107–124.

Karageorgiou V, Kaplan D. 2005. Porosity of 3D biomaterial scaffolds and osteogenesis. Biomaterials 26:5474–5491.

Kweon H, Yoo MK, Park IK, Kim TH, Lee HC, Lee H, Oh J, Akaike T, Cho C. 2003. A novel degradable polycaprolactone networks for tissue engineering. Biomaterials 24:801–808.

Kim S, Ahn K, Park MS, Jeon O, Choi CY, Kim B. 2006. Poly(lactide-co-glycolide)/hydroxyapatite composite scaffolds for bone tissue engineering. Biomaterials 27:1399–1409.

Lampin M, Warocquier-Clérout R, Legris C, Degrange M, Sigot-Luizard MF. 1997. Correlation between substratum roughness and wettability, cell adhesion, and cell migration. J Biomed Mater Res 36:99–108.

Lange R, Lüthen F, Beck U, Rychly J, Baumann A, Nebe B. 2002. Cell-extracellular matrix interaction and physico-chemical characteristics of titanium surfaces depend on the roughness of the material. Biomol Eng 19:255–261.

Lebourg M, Serra RS, Estellés JM, Sánchez FH, Ribelles JLG, Antón JS. 2008. Biodegradable polycaprolactone scaffold with controlled porosity obtained by modified particle-leaching technique. J Mater Sci: Mater Med 19:2047–2053.

Lee PC, Naguib HE, Park CB, Wang J. 2005. Increase of open-cell content by plasticizing soft regions with secondary blowing agent. Polym Eng Sci 45:1441–1451.

Lode A, Bernhardt A, Gelinsky M. 2008. Cultivation of human bone marrow stromal cells on three-dimensional scaffolds of mineralized collagen: Influence of seeding density on colonization, proliferation and osteogenic differentiation. J Tissue Eng Regen Med 2:400–407.

Oh SH, Park K, Kim JM, Lee JH. 2007. In vitro and in vivo characteristics of PCL scaffolds with pore size gradient fabricated by a centrifugation method. Biomaterials 28:1664–1671.

Reverchon E, Cardea S, Rapuano C. 2008. A new supercritical fluid-based process to produce scaffolds for tissue replacement. J Supercr Fluids 45: 365–373.

Salerno A, Oliviero M, Di Maio E, Iannace S, Netti PA. 2007. Design and preparation of m-bimodal porous scaffold for tissue engineering. J Appl Polym Sci 106:3335–3342.

Salerno A, Iannace S, Netti PA. 2008. Open pore biodegradable foams prepared via gas foaming and microparticulate templating. Macromol Biosci 8:655–664.

Salerno A, Guarnieri D, Iannone M, Zeppetelli S, Di Maio E, Iannace S, Netti PA. 2009. Engineered μ-bimodal poly(ε-caprolactone) porous scaffold for enhanced hMSCs colonization and proliferation. Acta Biomater 5:1082–1093.

Salerno A, Oliviero M, Di Maio E, Netti PA, Rofani C, Colosimo A, Guida V, Dallapiccola B, Palma P, Procaccini E, Berardi AC, Velardi F, Teti A, iannace S. 2010. Design of novel three-phase PCL/TZ-HA biomaterials for use in bone regeneration applications. J Mater Sci: Mater Med 21:2569–2581.

Sang VL, Bhatia SN. 2004. Three-dimensional tissue fabrication. Adv Drug Deliv Rev 56:1635–1647.

Silva MMCG, Cyster LA, Barry JJA, Yang XB, Oreffo ROC, Grant DM, Scotchford CA, Howdle SM, Shakesheff KM, Rose FRAJ. 2006. The effect of anisotropic architecture on cell and tissue infiltration into tissue engineering scaffolds. Biomaterials 27:5909–5917.

Sosnowski S, Woźniak P, Lewandowska-Szumiel M. 2006. Polyester scaffolds with bimodal pore size distribution for tissue engineering. Macromol Biosci 6:425–434.

Vidaurre A, Castilla Cortázar I, Gómez Ribelles JL. 2007. Polymeric scaffolds with a double pore structure. J Non-Crystall Solids 353:1095–1100.

Wei G, Ma PX. 2004. Structure and properties of nano-hydroxyapatite/polymer composite scaffolds for bone tissue engineering. Biomaterials 25:4749–4757.

Yao D, Smith A, Chaudhry GR, Nagarajan P, Vasquez A, Dang L. 2006. Fabrication of polycaprolactone scaffolds using a sacrificial compression-molding process. J Biomed Mater Res B: Appl Biomater 77B:287–295.

Ye L, Zeng X, Li H, Wang Z. 2010. Fabrication and biocompatibility of porously bioactive scaffold of nonstoichiometric apatite and poly(ε-caprolactone) nanocomposite. J Appl Polym Sci 116:762–770.

Yoshida T, Kikuchi M, Kyama Y, Takakuda K. 2010. Osteogenic activity of MG63 cells on bone-like hydroxyapatite/collagen nanocomposite sponges. J Mater Sci Mater Med 4:1263–1272.